

SUBSTELLAR OBJECTS IN NEARBY YOUNG CLUSTERS (SONYC) VI:  
THE PLANETARY-MASS DOMAIN OF NGC1333ALEXANDER SCHOLZ<sup>1</sup>, RAY JAYAWARDHANA<sup>2,\*\*</sup>, KORALJKA MUZIC<sup>2</sup>, VINCENT GEERS<sup>3</sup>, MOTOHIDE TAMURA<sup>4</sup>, ICHI TANAKA<sup>5</sup>*To appear in ApJ*

## ABSTRACT

Within the SONYC – *Substellar Objects in Nearby Young Clusters* – survey, we investigate the frequency of free-floating planetary-mass objects (planemos) in the young cluster NGC 1333. Building upon our extensive previous work, we present spectra for 12 of the faintest candidates from our deep multi-band imaging, plus seven random objects in the same fields, using MOIRCS on Subaru. We confirm seven new sources as young very low mass objects (VLMOs), with  $T_{\text{eff}}$  of 2400–3100 K and mid-M to early-L spectral types. These objects add to the growing census of VLMOs in NGC1333, now totaling 58. Three confirmed objects (one found in this study) have masses below  $15 M_{\text{Jup}}$ , according to evolutionary models, thus are likely planemos. We estimate the total planemo population with  $5\text{--}15 M_{\text{Jup}}$  in NGC1333 is  $\lesssim 8$ . The mass spectrum in this cluster is well approximated by  $dN/dM \propto M^{-\alpha}$ , with a single value of  $\alpha = 0.6 \pm 0.1$  for  $M < 0.6 M_{\odot}$ , consistent with other nearby star forming regions, and requires  $\alpha \lesssim 0.6$  in the planemo domain. Our results in NGC1333, as well as findings in several other clusters by ourselves and others, confirm that the star formation process extends into the planetary-mass domain, at least down to  $6 M_{\text{Jup}}$ . However, given that planemos are 20–50 times less numerous than stars, their contribution to the object number and mass budget in young clusters is negligible. Our findings disagree strongly with the recent claim from a microlensing study that free-floating planetary-mass objects are twice as common as stars – if the microlensing result is confirmed, those isolated Jupiter-mass objects must have a different origin from brown dwarfs and planemos observed in young clusters.

*Subject headings:* stars: formation, low-mass, brown dwarfs – planetary systems

## 1. INTRODUCTION

The frequency of free-floating objects with masses below the Deuterium burning limit ( $< 0.015 M_{\odot}$ ) – in the following called ‘planemos’, short for planetary-mass objects – is a subject of debate in the literature. Deep surveys in nearby star forming regions indicate the presence of at least some planemos (e.g. Tamura et al. 1998; Zapatero Osorio et al. 2000; Lucas & Roche 2000; Jayawardhana & Ivanov 2006; Luhman et al. 2008; Marsh et al. 2010a), but they yield conflicting results regarding their numbers. On the other hand, a recent micro-lensing study (Sumi et al. 2011) reports the presence of a large population of Jupiter-mass objects in the field (‘almost twice as common as stars’), which are either without host star or on very wide orbits. Direct detections of field objects in this mass domain have been reported as well (e.g. Liu et al. 2011; Leggett et al. 2012). So far, it is unclear whether the mass function declines in the planemo domain or not. Young planemos are also useful as benchmark objects for testing models for atmospheres and evolution in a

new mass and age domain.

One of the goals of our SONYC survey (short for Substellar Objects in Nearby Young Clusters) is to probe the planemo domain in several nearby star forming regions, using broadband imaging surveys followed by spectroscopic verification of the candidates. One of our targets is the young cluster NGC1333, a  $\sim 1$  Myr old compact star forming region in the Perseus OB association (see Fig. 1). In this cluster we found a rich substellar population, with about 30–40 brown dwarfs (Scholz et al. 2009, hereafter SONYC-I). In our most recent paper on this cluster we also report the discovery of a handful of objects with estimated masses below  $0.02 M_{\odot}$ , one of them at roughly  $0.006 M_{\odot}$  and thus firmly in the planemo regime (Scholz et al. 2012a, hereafter SONYC-IV).

Thus far, the number of planemos in this cluster seems low compared with other regions. This, however, is a preliminary result, for two reasons: 1) Our spectroscopic follow-up was not sufficiently complete in the planemo domain. 2) Our optical survey might not be sufficiently deep in some of the parts of NGC1333 subject to high attenuation due to reddening. Here we aim to resolve these issues through additional spectroscopy of faint candidates and a cumulative analysis, thus providing more definitive constraints on the planemo population of this cluster.

## 2. TARGET SELECTION

The goal of this paper is to probe specifically the planemo regime in NGC1333 and to address the potential biases outlined in Sect. 1. To that end, we selected three samples of objects for follow-up spectroscopy, in

Electronic address: alexs@cp.dias.ie

<sup>1</sup> School of Cosmic Physics, Dublin Institute for Advanced Studies, 31 Fitzwilliam Place, Dublin 2, Ireland

<sup>2</sup> Department of Astronomy & Astrophysics, University of Toronto, 50 St. George Street, Toronto, ON M5S 3H4, Canada

<sup>3</sup> Institute for Astronomy, ETH Zurich, Wolfgang-Pauli-Strasse 27, 8093 Zurich, Switzerland

<sup>4</sup> National Astronomical Observatory, Osawa 2-21-2, Mitaka, Tokyo 181, Japan

<sup>5</sup> Subaru Telescope, National Astronomical Observatory of Japan, 650 North A’ohoku Place, Hilo, HI 96720, USA

<sup>\*\*</sup> Principal Investigator of SONYC

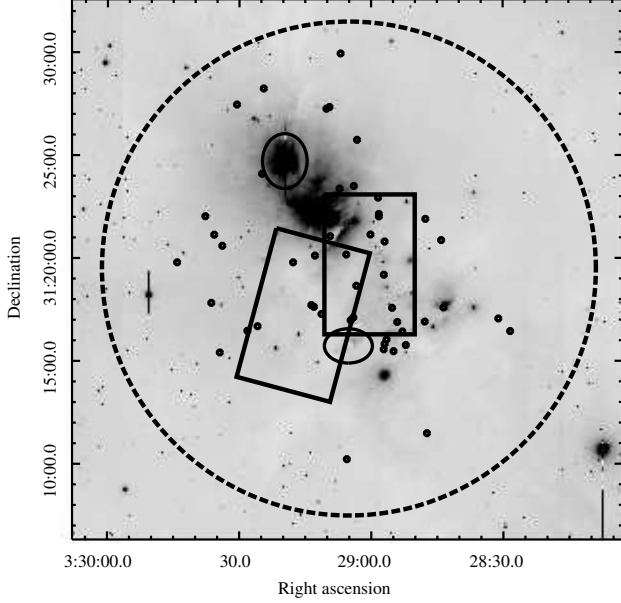


FIG. 1.— Subaru/Suprime-Cam i-band image for our target region NGC 1333 in the Perseus star-forming region. This image is identical to Fig. 1 in Scholz et al. (2012a), but we have overplotted with solid lines the two MOIRCS fields observed for this paper. Marked are the cluster radius with a large dashed circle, the two well-known objects BD+30 549 (north) and HH 7-11 (south) with small ellipses, and the known population of very low mass members (Scholz et al. 2009) with small circles. The reflection nebula NGC 1333 is slightly north of the image center. Coordinates are J2000.

total 19 objects, which are listed in Tables 1 and 2.

1. *IZ candidates:* Here we started with our primary set of 196 candidates identified based on the  $(i, i-z)$  colour-magnitude diagram (SONYC-I). This diagram is shown in Fig. 2; objects for which we previously obtained spectra are marked with crosses, confirmed very low mass objects with squares. A subsample of 22 objects with  $i > 22$  has not yet been verified spectroscopically. 20 of these objects are within  $0.25^\circ$  of the cluster center, which is the area where all confirmed very low mass members are located. From these 20, we select 6 for follow-up spectroscopy, marked with triangles in Fig. 2. As can be seen in the figure, these candidates cover  $i$ -band magnitudes from 22.5 to 25, extending beyond the nominal completeness limit of the photometric survey (dashed line). Including this new selection, 27 out of 43 IZ candidates with  $i > 22$  and 9 out of 15 with  $i > 24$  have been observed spectroscopically. The lowest mass confirmed member of the cluster, SONYC-NGC1333-36, with an estimated mass of  $0.006 M_\odot$  appears in this plot at  $i = 23.39$  and  $i - z = 1.96$ .

2. *JKS candidates:* We correlated the deep JK catalogue presented in SONYC-I with the 'HREL' catalogue from the Spitzer 'Cores to Disks' (C2D) legacy program (Evans et al. 2009). We accepted a source if it has a Spitzer counterpart within  $1''$  and uncertainties below  $0.2 \text{ mag}$  in the first two IRAC bands at  $3.6$  and  $4.5 \mu\text{m}$  (hereafter  $I_1$  and  $I_2$ ). This yields a catalogue of 824 objects (called the JKS catalogue). The  $(J, I_1-I_2)$  colour-magnitude diagram for this sample is plotted in Fig. 3. The figure illustrates that this catalogue is significantly deeper than the IZ selection: the faintest IZ candidates

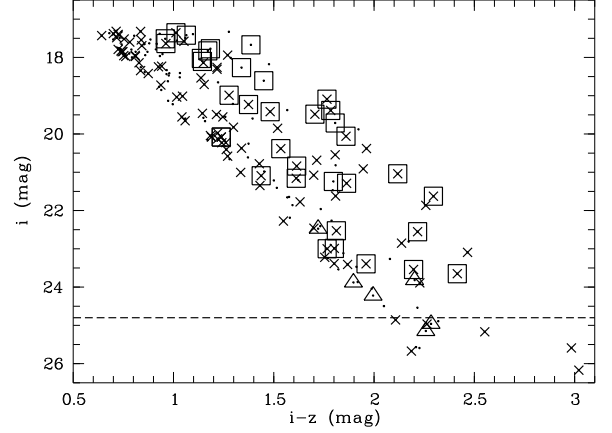


FIG. 2.— Colour-magnitude diagram for the  $iz$  candidates (dots), originally identified in SONYC-I. The figure is identical to Fig. 7 in SONYC-IV, but we have also marked the candidates targeted in the new campaign with triangles. Crosses are objects for which we have already obtained spectra in previous campaigns. Confirmed very low mass objects are marked with squares. The horizontal dashed line shows the completeness limit of the photometric survey as estimated in SONYC-I.

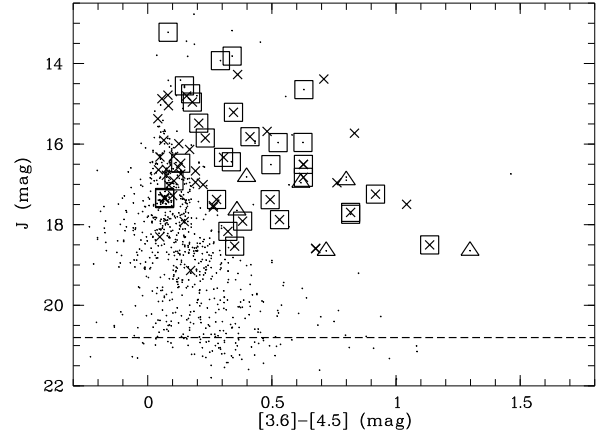


FIG. 3.— Colour-magnitude diagram for the JKS candidates (dots), see text for details. Confirmed very low mass objects are marked with squares, crosses are objects for which we have already obtained spectra in previous campaigns. Objects targeted in this new campaign are marked with triangles. The completeness limit of the J-band photometry is marked with a dashed line.

have  $J \sim 19$ , whereas the JKS catalogue is complete down to  $J = 20.8$ . From this catalogue, we only consider the subsample with  $I_1 - I_2 > 0.3$ . This cut-off was introduced to avoid the bulk of the datapoints in the diagram, for which a spectroscopic follow-up is not practical; in Sect. 5.3 we will discuss the consequences of this cut on the completeness of the survey. There are only 17 objects without spectroscopic verification with  $16 < J < 19$ ,  $I_1 - I_2 > 0.3$  and (as above) a distance from the cluster center below  $0.25^\circ$ . Out of these 17, we selected 6 for follow-up spectroscopy, which are marked with triangles. The aforementioned SONYC-NGC1333-36 appears in this plot at  $J = 18.53$  and  $I_1 - I_2 = 0.35$ . Note that spectroscopic verification for objects beyond  $J = 19$  is not feasible with the currently available facilities.

3. *Random candidates:* After selecting the IZ and JKS candidates, we decided to observe two MOIRCS fields

(see Sect. 3 and Fig. 1), which cover a large fraction of the samples. To prepare the spectroscopy run, we took a new set of deep K-band images for these two fields. From these images, we selected 7 more sources for spectroscopy, for which we had no prior information about their colours. The only constraint for these random sources was the outline of the slit mask.

We note that most of the selected objects are listed as candidates from photometric surveys in the literature, in papers by Aspin et al. (1994); Lada et al. (1996); Wilking et al. (2004); Oasa et al. (2008); Gutermuth et al. (2008).

Two caveats need to be pointed out with regard to the selection of candidates from colour-magnitude diagrams, as done here for the IZ and JKS candidates.

First, the completeness of the survey depends strongly on the definition of the colour and magnitude criteria used to select the candidates for follow-up spectroscopy. For the IZ sample, we defined the selection box based on the position of previously identified brown dwarfs and extend it at the faint end – we are simply probing the extension of the colour space occupied by the known brown dwarfs towards fainter magnitudes. A similar strategy was used for the JKS sample, but as argued above, we need to introduce an additional colour cut (see also the discussion Sect. 5.3). In the two samples, the colour cuts are independent of evolutionary models.

Second, the photometric uncertainties may cause us to miss some brown dwarfs. For the IZ selection, this is not a major problem: The median error (excluding systematics) for  $i > 22$  is 0.05 mag, and 95% of the errors are below 0.1 mag. The width of the selection box (1 mag in (i-z) colour) is significantly larger than the errors. In addition, most of the confirmed objects are 0.1-0.2 mag to the right side of the left boundary of the box. Assuming that these objects show a reliable representation of the cluster isochrone in NGC1333, even large uncertainties are unlikely to move the datapoints of substellar members out of our selection box. Note that the right side of our selection criterion was only formal, no objects in our survey had colours redder than this boundary.

In the JKS sample, the median error in the (I1-I2) colour is 0.1 mag for  $16 < J < 19$ . For  $18 < J < 19$ , i.e. at the faint end of our candidate selection, the errors are  $\leq 0.22$  mag. These errors do not depend significantly on the (I1-I2) colour. The expected (I1-I2) colours of brown dwarfs and planemos are close to the bulk of the datapoints in this diagram (see Sect. 5.3), i.e. we may lose objects on the left side of our colour cut due to large photometric errors.

### 3. OBSERVATIONS AND DATA REDUCTION

New spectra for candidate planemo members of NGC1333 were taken using the near-infrared spectrograph MOIRCS at the Subaru telescope in multi-object (MOS) mode. Since our targets are faint and require long integration times, MOS is the most practical way of conducting a spectroscopic survey. After creating the IZ and JKS candidate samples, we looked for the optimum way to obtain spectra for as many as possible of these objects. We found that two MOIRCS fields arranged as shown in Fig. 1 can cover 12 of these candidates (6 IZ and 6 JKS, as discussed in Sect. 2).

K-band pre-imaging was carried out for these fields in

September 2011, with excellent seeing (0.3") and under good conditions. The pre-images were reduced and calibrated using 2MASS photometry. Aperture magnitudes were measured for all our candidates, to complement and verify the available photometry. These pre-images are used to define the masks for the spectroscopy run, which was carried out in the night of Nov 14-15. For most of this night, we observed under stable conditions and with seeing in the range of 0.5". At 2am local time, about 2 hours before the end of the visibility for our target region, the humidity increased above 80% forcing us to close the dome. In total, we spent 3:20h telescope time on mask 1 and 3:10h on mask 2. At the beginning of the night and between mask 1 and mask 2 we observed 3 standard stars with spectral type around A0 intended to be used for telluric calibration.

We used our two MOS masks, the grism HK500 with a nominal resolution of 600-800 and a wavelength coverage from 1.3 to 2.4  $\mu m$ , an order sorting filter, and slits with a length of 11.7" and a width of 1.17". For each mask we obtained a series of individual exposures of at most 5 min. Due to an incident with the spillage of cooling liquid earlier in the year (July 2 2011), the autoguider system was not operational at the time of the observations. Therefore, we checked the position of the mask alignment stars between individual exposures and re-aligned the mask if the offset was more than the typical seeing in the direction perpendicular to the slit. If the offsets were large, we reduced the integration time to be able to track the sources reliably. The mask position was typically stable over several minutes, the integration times for individual exposures were 240 sec for mask 1 and 80-300 sec for mask 2. The total on-source time was 88 min for mask 1 and 60 min for mask 2. Between consecutive exposures, the telescope was nodded along the slits by 2".

We reduced the MOIRCS spectra using the recipes described in detail in SONYC-I. This includes the a) subtraction of consecutive exposures that are offset along the slit, b) division by a normalised domeflat calculated from lamp-on and lamp-off exposures, and c) the stacking of the individual frames for each mask. For the last step, we measured the position of one of the sources in the slit for each individual frame and shifted the frames accordingly, to account for small offsets.

Spectra were extracted using *apall* in IRAF. This includes aperture definition, background subtraction, and trace fitting. We opted for a full aperture integration across the profile (as opposed to optimum extraction), because many of our sources are faint and lack a well-defined profile. The same procedure was carried out for the standard stars. The wavelength solution was determined from  $\sim 10$  telluric lines in the raw spectra. For each target, the two resulting spectra, corresponding to the two positions in the slit, were coadded. The final spectra are re-binned to 40Å per wavelength element.

The three standards HIP6855, HIP9196, and HIP21115 have been observed at airmasses of 1.46, 1.64 and 1.10, while the average airmass for the science exposures was 1.30 for mask 1 and 1.06 for mask 2. The spectrum for HIP6855 has a significantly lower flux level in the K-band (by 10-20%) than the two other stars and was not used. The scaled spectra for HIP9196 and HIP21115, however, are very similar with small differences in the range of 1-2%, well-explained by the differences in air-

mass. This is consistent with an extinction coefficient difference (mag/airmass) in the range of 0.01 between H- and K-band, which is plausible for Mauna Kea.

Because HIP21115 was observed between the two masks and thus should give the best approximation to the conditions during the science exposures, we used its spectrum for the calibration. All science spectra were divided by the quotient between the telluric standard spectrum and the tabulated spectrum of an A0 star (Pickles 1998).<sup>7</sup>

#### 4. SPECTRAL ANALYSIS

The 19 available spectra were analysed using the recipes described in detail in SONYC-IV. In the following, we give a brief summary of the four steps and describe the results.

1. *Selection of young very low mass objects:* 7 spectra show the characteristic spectral signature of young very low mass objects. Specifically, they exhibit the sharp 'H-band peak' at  $1.68\ \mu\text{m}$  caused by broad water absorption features at  $1.3\text{--}1.5$  and  $1.75\text{--}2.05\ \mu\text{m}$  (Cushing et al. 2005), which is an indication for low-gravity (Brandeker et al. 2006). These 7 sources are considered to be very low mass objects. Given the compact nature of NGC1333 and the low space densities for these objects (Caballero et al. 2008), contamination by foreground or background objects is negligible. Thus, these 7 objects are most likely young members of NGC1333. Their spectra are shown in Fig. 4; their properties listed in Table 1. The remaining 12 spectra are either featureless or show only little structure in the H-band. They are listed in Table 2.

2. *Spectral types:* For the 7 objects from Table 1 we measured spectral types using the H-peak index (hereafter HPI) introduced in SONYC-IV, after dereddening the spectra using the spectroscopic  $A_V$  (see below). As discussed in the previous paper, other near-infrared indices suggested in the literature are not suitable for our type of data. The HPI calculates the flux ratio between the wavelength intervals  $1.68$  and  $1.50\ \mu\text{m}$  and is usable for  $>\text{M6}$  spectral types. Using the calibration given in SONYC-IV, all 7 objects identified here have spectral types of M7 or later (see Table 1), the latest type is  $\sim\text{L1}$  (albeit with a noisy spectrum). The typical uncertainty is one subtype.

3. *Effective temperatures:* We calculate a grid of model spectra for effective temperatures from  $1500$  to  $3900\ \text{K}$  (in steps of  $100\ \text{K}$ ) and extinctions  $A_V$  from  $0$  to  $30\ \text{mag}$ . This grid is based on the DUSTY models by Allard et al. (2001). For all objects with any indication of structure in the H-band, we searched for the best matching model spectrum. This was done in the following way: For each model we subtracted observed spectrum from model spectrum, squared this quantity, divided by the model spectrum, and averaged the residual over the wavelength domain  $1.38\text{--}1.78$  and  $2.10\text{--}2.32\ \mu\text{m}$ . We selected the model spectrum for which this quantity is minimal, and adopted its parameters as best fit (see Table 1). The typical uncertainty is  $\pm 200\ \text{K}$  in  $T_{\text{eff}}$  and  $\pm 1\ \text{mag}$

<sup>7</sup> Although HIP21115 is a B9V star, we used the tabulated A0 spectrum because the Pickles et al. spectrum for spectral type A0 has much better resolution. The difference in the flux levels between A0 and B9 do not matter in the H- and K-band for our purposes.

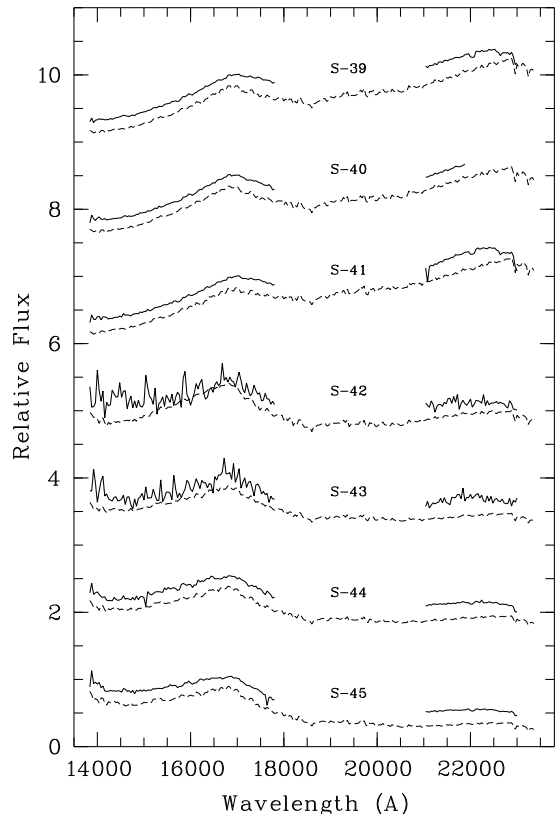


FIG. 4.— Near-infrared spectra of the 7 newly identified very low mass members of NGC1333 (solid lines). The dashed lines show the best-fitting, reddened model spectra with the parameters as listed in Table 1. The spectra are offset on the y-axis by constants for clarity.

in  $A_V$ . Whenever possible we also calculated  $A_V$  from the J- and K-band photometry. The results are given in Table 1. The 7 very low mass objects have effective temperatures between  $2400$  and  $3100\ \text{K}$ . The remaining sources with recognisable structure in the H-band have temperature around or above  $3500\ \text{K}$  (Table 2). The object SONYC-NGC1333-42, the coolest source in our sample, has a noisy spectrum; therefore we manually chose the best-fitting model. The best-fitting reddened models are overplotted in Fig. 4.

Two of the objects in Table 1 were selected randomly. One of them (SONYC-NGC1333-45) turns out to be on our initial list of IZ candidates but much brighter than the cutoff used for this paper ( $i = 18.609$  vs.  $i = 22$ ). It was previously confirmed by Winston et al. (2009). They find a spectral type of M8 and a temperature of  $2700\ \text{K}$ ; our analysis yields consistent results (M8 and  $2900\ \text{K}$ ). The second random source, SONYC-NGC1333-44, has been listed before as a photometric candidate (Aspin et al. 1994; Oasa et al. 2008). It was not found in our IZ survey because it sits very close to a blooming spike caused by a bright star.

4. *Sanity checks:* As in our previous papers, we additionally compared the spectra to literature spectra of other brown dwarfs. This is particularly important to make sure that our results are not severely affected by the often low signal-to-noise ratio in our data. For comparison we use the spectra for the three young

TABLE 1  
NEW VERY LOW MASS MEMBERS OF NGC1333

ID	$\alpha$ (J2000)	$\delta$ (J2000)	J (mag)	K (mag)	SpT	$A_V$ (phot)	$A_V$ (spec)	$T_{\text{eff}}$	Comments
39	03:28:54.96	+31:18:15.3	16.881	13.155	M8.5	15	17	2900	IZ
40	03:29:02.80	+31:22:17.3	16.959	13.423	M9.3	14	15	2700	JKS
41	03:29:04.63	+31:20:28.9	17.647	13.892	M7.6	15	18	3100	JKS
42	03:29:13.85	+31:18:05.7	19.252	17.540	L1	4	4	2400	IZ <sup>a</sup>
43	03:29:21.94	+31:18:29.2	18.728	17.128	M8.1	3	5	2900	IZ
44	03:28:57.04	+31:16:48.7	—	15.59	M8.6	—	4	2800	random
45	03:29:13.04	+31:17:38.3	15.23	14.16	M8.1	0	2	2900	random

<sup>a</sup> Fit manually adjusted to account for poor spectral quality

TABLE 2  
OBJECTS RULED OUT AS VERY LOW MASS  
MEMBERS OF NGC1333

$\alpha$ (J2000)	$\delta$ (J2000)	Comments
03:29:04.31	+31:19:06.4	JKS, $T \sim 3500$
03:28:59.33	+31 16 31.5	IZ, $T > 3500$
03:29:01.88	+31:16:53.4	JKS, $T \sim 3500$
03:29:02.69	+31 19 05.6	IZ, $T \sim 3500$
03:28:58.42	+31:22:17.6	JKS, featureless
03:29:05.67	+31:21:33.9	JKS, $T \sim 3500$
03 29 13.05	+31 16 39.8	IZ, $T > 3500$
03:29:00.02	+31:17:13.4	random, $T > 3500$
03:28:56.31	+31:20:35.2	random, featureless
03:29:06.45	+31:16:52.0	random, featureless
03:29:16.26	+31:18:06.6	random, featureless
03:29:21.88	+31:17:40.7	random, featureless

objects 2M1207 A, DH Tau B, and 2M1207 B, published by Patience et al. (2012) in a detailed comparison with model spectra. For all three they find a satisfying match with different types of model spectra and consistent temperatures for a variety of spectral ranges and model spectra. According to their analysis, these objects have effective temperatures of 3100, 2600, and 1600 K, when HK spectra are compared with DUSTY models, which is comparable to the way we have determined temperatures. With our method, we derive  $T_{\text{eff}}$  of 3200, 2800, and 1700 K for the same data, consistent with the published values.

In Fig. 5 we plot their spectra in comparison with three of our newly identified objects in NGC1333 with similar temperatures: SONYC-NGC1333-41, -40, and -42 with  $T_{\text{eff}}$  of 3100, 2700 and 2400 K. The SONYC spectra were dereddened using the spectroscopic  $A_V$  given in Table 1. From Fig. 5 it seems plausible that the two pairs SONYC-NGC1333-41/2M1207 A and SONYC-NGC1333-40/DH Tau B have similar temperatures. Based on the slope of the H-band peak, it is also justified to say that SONYC-NGC1333-42 is probably somewhat hotter than 2M1207 B. There are some offsets in the flux level in the K-band, which may be explained by inaccuracies in the extinction and/or excess flux from a disk. Overall, the results of our analysis are confirmed.<sup>8</sup>

For the same three new SONYC objects, we compare the photometric fluxes from 0.8 to  $8 \mu\text{m}$ , as far as avail-

<sup>8</sup> The study by Patience et al. (2012) includes three more young sources – CT Cha, GQ Lup B, TWA5 B. For these objects their comparison with models does not yield consistent temperatures and the fit with the model spectra is poor. Therefore we do not use them for the comparison, but these objects clearly pose a challenge for our understanding of substellar spectra.

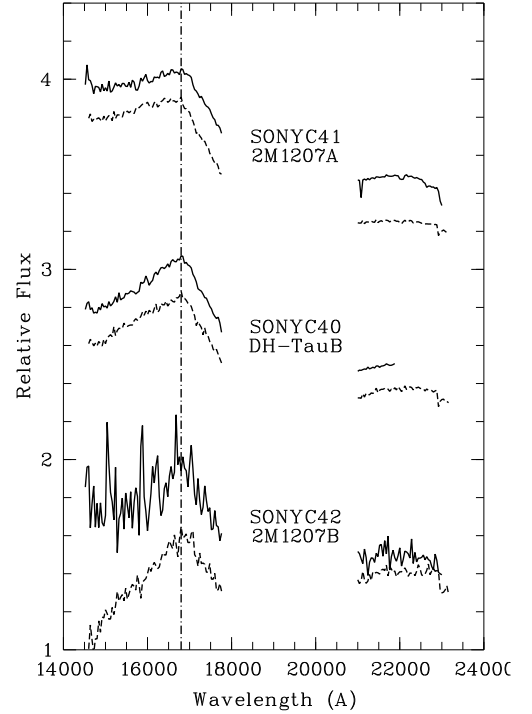


FIG. 5.— Three spectra for newly identified very low mass members of NGC1333 from Table 1 (solid lines) in comparison with published spectra for brown dwarfs from Patience et al. (2012) with similar effective temperature (dashed lines). The spectra are offset on the y-axis by constants for clarity.

able, with the model spectra, adopting  $T_{\text{eff}}$  and the photometric  $A_V$  as listed in Table 1, see Fig. 6. Again, this comparison confirms the results from our analysis. For SONYC-NGC1333-40 mid-infrared excess is clearly visible and can be attributed to the presence of a disk. As pointed out in SONYC-IV, spectroscopy covering the wide spectral range from the J- to the M-band promises to be the ideal tool to improve the characterisation of substellar objects.

## 5. DISCUSSION

With the new spectra presented in this paper we have enlarged the number of known very low mass members in NGC1333. In SONYC-IV we list 51 confirmed objects with spectral type M5 or later and/or effective temperature of 3200 K or lower (41 previously known and 10 new); this new campaign adds 7 new objects to this census. Based on the currently available isochrones for this mass domain, most of these 7 are cool enough to be considered to be brown dwarfs. In the following we will

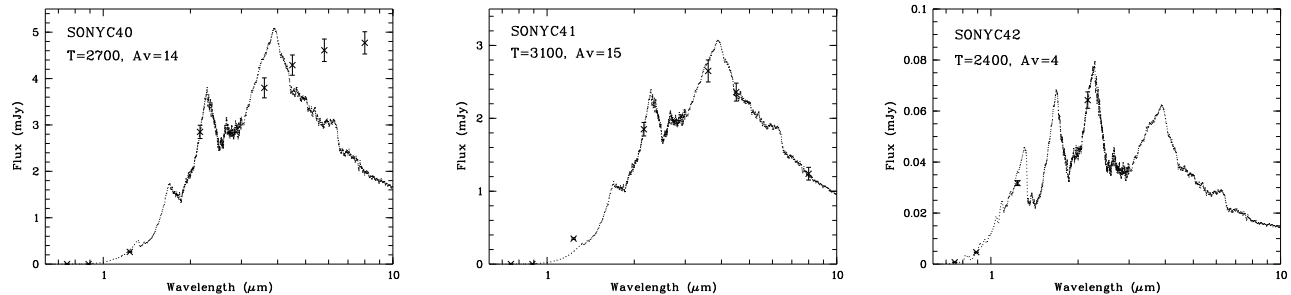


FIG. 6.— Photometric spectral flux distribution for three newly identified very low mass members of NGC1333 in comparison with DUSTY model spectra for  $T_{\text{eff}}$  as given in Table 1. The model spectra have been dereddened using the photometric  $A_V$  listed in Table 1.

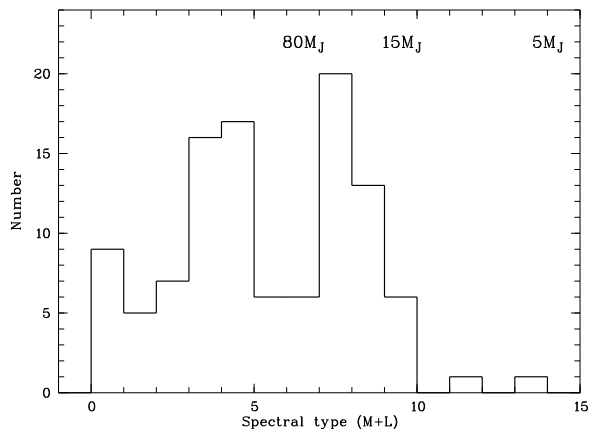


FIG. 7.— Distribution of spectral types for the very low mass population in NGC1333, including the previously confirmed objects with  $\geq M5$  listed in SONYC-IV, the new objects found in SONYC-IV and this paper, and the earlier type objects classified in Winston et al. (2009). Note that Winston et al. additionally classify 12 objects with spectral types earlier than M0. Approximate mass limits according to DUSTY/COND isochrones are given.

discuss the implications of the new results for the substellar population in NGC1333, with particular focus on the planemo domain.

### 5.1. The distribution of spectral types and magnitudes

We begin by showing the spectral type distribution for all spectroscopically classified M and L-type objects in NGC1333 in Fig. 7. This includes the very low mass objects listed in SONYC-IV, new objects identified in the same paper and this new study, plus earlier type objects classified in Winston et al. (2009). Their spectroscopic survey is essentially complete down to the brown dwarf/star boundary (for  $A_V < 10$ ), and thus ideally complements our own studies, which are not complete above the substellar boundary.

For the stellar regime, the distribution of spectral types in NGC1333 resembles those found for other regions (ChaI, IC348, Taurus, see Luhman 2007), with a peak around M4 and a increase in the frequency between M0 and M5 by about a factor of 3. For later spectral types, we observe a second peak around M7, which is not seen in these three other regions.

Another relevant feature in the context of this paper is the sharp drop of the numbers at M9. Based on the COND (Baraffe et al. 2003) and DUSTY (Chabrier et al. 2000) isochrones, M9 corresponds to a mass around the Deuterium burning limit. Only two objects (SONYC-NGC1333-36 at  $\sim L3$  and SONYC-NGC1333-42 at  $L1$ )

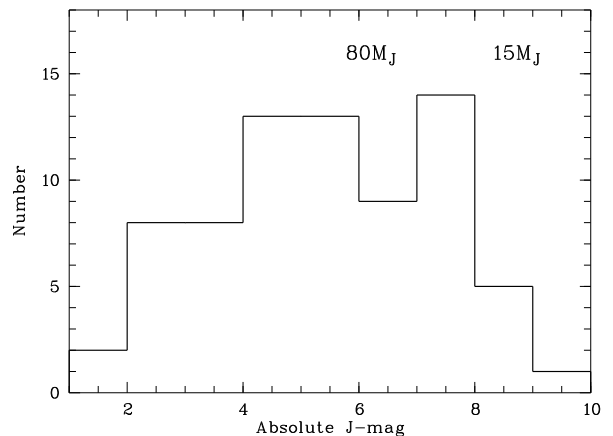


FIG. 8.— Distribution of absolute J-band magnitudes for the Class II in NGC1333 from Gutermuth et al. (2008) for all sources with  $A_V < 10$ . Approximate mass limits according to DUSTY/COND isochrones are given.

have later spectral types. Thus, the number of observed planemos in this cluster is very low. This feature will be further discussed in the following subsections.

As an independent check of the distribution shown in Fig. 7, we examine the histogram of absolute J-band magnitudes for the population of Class II sources in NGC1333, as identified by Gutermuth et al. (2008) based on Spitzer data. Of their 137 objects, 94 have photometry in 2MASS. We calculate  $A_V$  from J- and K-band photometry, using the same prescription as in SONYC-IV, deredden the J-band photometry and subtract the distance modulus of 7.4 (assuming a distance of 300 pc, see Belikov et al. 2002). We exclude the most reddened objects and consider only the 74 with  $A_V < 10$ . In this extinction regime the distribution of J-band magnitudes does not show a dependence on  $A_V$ .

Fig. 8 shows again a peak slightly above the substellar limit, which corresponds to the peak around M4-M5 in the spectral type distribution. A second peak is visible in the substellar regime (for  $M_J$  of 7-8), but it is much less pronounced than the peak at M7 seen in Fig. 7. In fact, within the statistical errors the magnitude distribution is consistent with a broad peak around  $M_J = 5$  and a decline at fainter magnitudes, which agrees with previously published results for Cha-I and IC348 (Luhman 2007). Thus, the second peak in the spectral type distribution could be spurious. One possible explanation is a gap in completeness between the spectroscopic samples from Winston et al. (2009) and ours, causing us to miss objects at  $\sim M6$ .

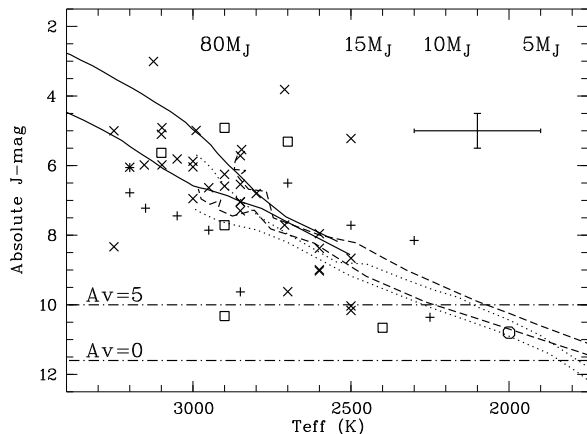


FIG. 9.— HRD for the very low mass population in NGC1333 (crosses – previously known objects in the census from SONYC-IV, pluses – new objects found in SONYC-IV, squares – new objects identified in this paper). The circle shows the improved parameters for SONYC-NGC1333-36 after fitting the photometric SED, see SONYC-IV. Model isochrones (solid – BCAH, dotted – DUSTY, dashed – COND) are shown for 1 (upper) and 5 Myr (lower). The dash-dotted lines show the limits of our spectroscopic survey for  $A_V = 0$  and 5 mag.

### 5.2. The Hertzsprung-Russell diagram

In Fig. 9 we show the HRD for NGC1333, focusing on the very low mass objects with spectral types of M5 or later. Out of the 41 previously known sources listed in SONYC-IV (crosses), the 10 newly identified in SONYC-IV (pluses), and the 7 newly identified in this paper (squares), 51 have estimated effective temperatures and are plotted in the figure.

Instead of luminosity, we prefer to plot the absolute J-band magnitude to avoid additional errors from the bolometric correction. The absolute J-band magnitudes are calculated in the same way as in Sect. 5.1, including dereddening of the J-band data<sup>9</sup> and subtraction of the distance modulus. The typical errorbar in the absolute J-band magnitude is  $\pm 0.5$  mag, which combines the errors in  $A_V$  ( $\pm 1$  mag), distance ( $\pm 20$  pc), and photometry (up to  $\pm 0.1$  mag). The uncertainty in effective temperature, as outlined above, is  $\pm 200$  K. The approximate mass limits according to the DUSTY and COND isochrones, assuming an age of 1 Myr, are given as well.

The general trend in this diagram is in good agreement with 3 sets of isochrones from the Lyon group: DUSTY, COND, and BCAH (Baraffe et al. 1998). Typical for HRDs of star forming regions, the objects show a large spread due to various effects (e.g. Littlefair et al. 2011). However, only 7 objects (14%) are inconsistent with the 1-5 Myr isochrones within the errorbars. Some of them could be affected by ongoing accretion or strong magnetic activity (overluminosity) – see Scholz et al. (2012b) for a discussion – or grey extinction by an edge-on disk (underluminosity). Some might experience variability (Scholz 2012). In addition, there remains a small chance that an outlier is a fore- or background source: Perseus is known to have a complex substructure (Enoch et al.

2006; Ridge et al. 2006), i.e. there may be young objects at different distances. Moreover, in some cases the signal-to-noise in our spectra is not sufficient to confirm low gravity, i.e. we cannot completely exclude older objects in the field. Given these caveats, the overall agreement with the isochrones is good.

Only a very small number of 3 objects have temperature below 2500 K – SONYC-NGC1333-31, 36, and 42 – (two of them also with spectral type later than M9, see Sect. 5.1) and would have masses around or below the Deuterium burning limit. The plot demonstrates that the frequency of objects per bin in effective temperature drops significantly below 2500 K. There are 19 objects with  $2800 \leq T_{\text{eff}} < 3100$ , 13 with  $2500 \leq T_{\text{eff}} < 2800$ , but only 3 with  $2200 \leq T_{\text{eff}} < 2500$ . This confirms the finding from the spectral type distribution.

The drop in the frequency of observed objects below 2500 K and spectral type M9, already found in Sect. 5.1, can either be explained by an actual lack of planemos in this cluster, or by biases in our photometric survey and the selection of objects for follow-up spectroscopy, which will be discussed in the following subsection. In addition, there are three more caveats:

- 1) Extinction might limit the completeness of our survey below 2500 K. To test this, we have overplotted with dash-dotted lines the J-band limit of our survey ( $J = 19$ , see Sect. 2) for  $A_V = 0$  and  $A_V = 5$ . We should have been able to find objects with  $T_{\text{eff}} > 2200$  K and  $A_V \leq 5$ . The clear majority of the confirmed very low mass objects have  $A_V < 5$ . Also,  $A_V \sim 5$  is the median extinction for the sample of Class II objects published by Gutermuth et al. (2008), as far as their 2MASS photometry is available. Therefore we are unlikely to miss a significant number of planemos down to 2200 K due to their high extinction. For extinctions well below  $A_V$  of 5 mag we should be able to find sources even cooler than 2200 K (as proven by the detection of SONYC-NGC1333-36).

- 2) The isochrones might not accurately reflect the luminosity vs. effective temperature relation in young star forming regions. To explain a lack of planemos in Fig. 9, the isochrones would have to turn downwards below 2500 K, i.e. cooler objects need to be significantly fainter than expected based on these models. While this cannot be definitely excluded at the moment, the data for the eclipsing binary brown dwarf in Orion – currently the only available empirical test for these isochrones – does not indicate such a trend (Stassun et al. 2007). The luminosities for its components are in agreement with the predictions from the isochrones, in fact, for the lower mass component ( $M = 0.036 M_{\odot}$ ) the isochrone underestimates the luminosity, the reverse of what would be needed to explain the lack of planemos in NGC1333. Furthermore, it is difficult to conceive a significant departure from the smooth (almost linear) trend in the isochrones in Fig. 4, since this would require an additional and strong source of opacity in the J-band. To our knowledge, this is not born out by the available data, for example, the same isochrones fit the optical and near-infrared colours for the substellar population in  $\sigma$  Ori quite well down to the lowest masses (Caballero et al. 2007).

- 3) The effective temperatures – mostly determined with the routines used in this paper, i.e. by fitting DUSTY models to the near-infrared spectra – could be systematically unreliable in a way that  $T_{\text{eff}}$  is overesti-

<sup>9</sup> As in SONYC-IV, we use an intrinsic J-K colour of 1.0, which is roughly applicable down to the planemo regime. For comparison, the latest type objects in  $\sigma$  Ori (7 objects) have an average J-K of 1.25 (Caballero et al. 2007). A shift in  $J - K$  from 1.0 to 1.25 causes a shift of 1.36 mag in  $A_V$ .

ated for very cool sources. The study by Patience et al. (2012), already mentioned in Sect. 4, does not indicate any such trend. Specifically, their comparison the DUSTY models yield effective temperatures below 2000 K when compared with the spectra for 2M1207B, CT Cha B and GQ Lup B, three very young objects with L spectral types. This seems to work well even when only the H- and K-band spectra are considered, which is the case for our objects in NGC1333.

We conclude that these three caveats cannot be used to explain the lack of observed objects cooler than 2500 K and later than M9.

### 5.3. Survey completeness

In this subsection we will explore the possibility that our survey has missed a significant number of planemos due to a lack of depth or biases in the colour cuts.

Our initial candidate selection was based on a (i, i-z) colour magnitude diagram (the IZ catalogue, see Sect. 2). From the set of 196 candidates, more than half are now covered by follow-up spectroscopy. In particular, 27 out of 43 IZ candidates with  $i > 22$  and 9 out of 15 with  $i > 24$  have been verified spectroscopically. As illustrated in Fig. 2, the spectroscopy covers the entire colour-magnitude space of this selection down to the faint end. This candidate sample contains 2 likely planemos (SONYC-NGC1333-31 is not found in this survey). Statistically, the remaining candidates which have not been verified yet are expected to contain one more.

This selection, however, might have missed planemos, because the depth of the IZ survey is not sufficient. As argued in SONYC-IV, this is a distinct possibility; while the nominal completeness limit is  $i = 24.8$ , it might be lower in some parts of the cluster with strong background emission.

To overcome the depth limitation of the IZ survey, we have used the JKS catalogue, which contains all objects with J- and K-band photometry from our own survey and Spitzer photometry in the first two IRAC bands at 3.6 and 4.5  $\mu\text{m}$  (see Sect. 2). As illustrated in Fig. 3, this survey is much deeper and extends significantly beyond the limiting magnitude for follow-up spectroscopy ( $J = 19$ ). It should be complete down to  $J = 20.8$ . The near-infrared images do not show strong background structure due to the cloud, i.e. the completeness should be uniform across the cluster. The JKS catalogue contains about two thirds of the confirmed very low mass objects in NGC1333; most of the ones that are not in this catalogue are relatively bright and therefore affected by saturation in our deep near-infrared images. This catalogue contains 2 likely planemos (SONYC-NGC1333-42 does not have a Spitzer counterpart).

The colour-magnitude diagram from this catalogue is shown in Fig. 3. Our spectroscopic follow-up covers a large fraction of this diagram to the  $J = 19$  limit. According to the COND and DUSTY 1 Myr isochrones, this should correspond to a mass of 0.003-0.004  $M_{\odot}$  for  $A_V = 0$  and 0.006-0.008  $M_{\odot}$  for  $A_V = 5$ . For  $15 < J < 17$  the entire colour range in  $I1 - I2$  has been probed by spectroscopy; it turns out that most of the confirmed objects in this magnitude range (11/13) have  $I1 - I2 > 0.2$ . As the IRAC colour can be affected by excess emission due to a disk, this simply might reflect the high disk fraction in NGC1333 (see SONYC-IV). For

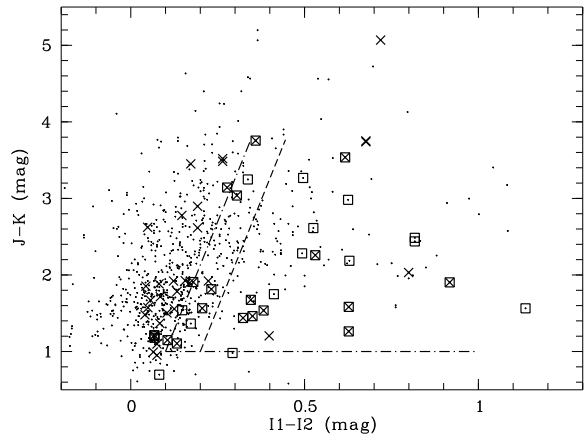


FIG. 10.— Colour-colour plot for the JKS catalogue (see Sect. 2). Marked are objects for which we have taken spectra (crosses) and confirmed very low mass members of NGC1333 (squares). The dash-dotted lines mark the colour space where brown dwarfs and planemos are expected to be found. The dashed line shows the reddening path for the average planemo.

$17 < J < 19$  we verified about three quarters of the objects with  $I1 - I2 > 0.3$ . Thus, in these colour domains the spectroscopic survey is sufficiently complete to rule out the existence of more than 1-2 additional planemos.

To further analyse the colour space from the JKS catalogue, we show a (J-K, I1-I2) colour-colour diagram in Fig. 10. In comparison with other colour combinations in this catalogue, this plot shows a relatively clear distinction between objects confirmed as very low mass cluster members and those rejected. All confirmed objects are marked with squares, all objects verified with spectroscopy with crosses. For this plot, we estimate the expected position of planemos based on the photometry of known young ultracool objects: In the  $\sigma$  Ori cluster (Scholz & Jayawardhana 2008) the average colour of 16 M9-L5-type objects is  $I1 - I2 = 0.2$ , albeit with a spread of  $\pm 0.2$  mag due to photometric uncertainties. Among 10 young field dwarfs with L0-L4 spectral type, the average colour is  $I1 - I2 = 0.17$  with a spread of 0.05 mag (Luhman et al. 2009). Based on these two samples, we adopt  $I1 - I2 = 0.2$  as typical intrinsic colour of planemos.

The dashed line in Fig. 10 shows the reddening path for  $A_V = 0 - 15$  starting with this intrinsic colour. Shifting this line by 0.1 mag to the left is in good agreement with the left boundary for most of the confirmed very low mass objects in NGC1333 (dash-dotted line). This line combined with a limit of  $J - K > 1.0$  is adopted as the colour space where brown dwarfs and planemos are expected.

In this regime we have 250 objects out of which 103 have  $16 < J < 19$  and are thus sufficiently faint to be planemos ( $J = 16$  corresponds to  $\sim 0.015 M_{\odot}$  for zero extinction in COND/DUSTY isochrones) and sufficiently bright to be accessible for spectroscopy. About one quarter of them has been observed spectroscopically. Thus, the catalogue could contain a few additional planemos – up to 6, statistically, which would yield a total of up to 8. This analysis shows that one particular bias in the selection of candidates, the cutoff at  $I1 - I2 = 0.3$  which was necessitated by the large amounts of contaminating



objects at bluer colours, might affect our ability to find planemos.

We should not miss any significant number of planemos with enhanced mid-infrared colours due to the presence of a disk. If the disk fraction for planemos is as high as for brown dwarfs, as shown for the  $\sigma$  Ori cluster (Scholz & Jayawardhana 2008), excess emission should be expected for about half of the planemos in NGC1333 (see SONYC-IV for more information on disk fractions). These objects should be located to the right of the dashed line. In this area we find 39 objects from which about half have been verified spectroscopically (including the two planemos). This implies that we might miss about two more objects in this colour domain. Assuming a disk fraction of around  $> 50\%$ , this again gives a total number of up to 8 planemos.

The JKS catalogue can further be used to probe the regime  $J > 19$  which is not accessible for spectroscopy. The JKS catalogue contains 292 objects with  $J > 19$ , 124 in the colour space expected for planemos (dash-dotted lines in Fig. 10). However, this sample is dominated by strongly reddened objects with high  $J - K$  colour. Only about 30 of them have  $J - K$  colours consistent with  $A_V < 5$  and only 7 are below  $A_V = 3$ . Given that two thirds of the confirmed brown dwarfs have an optical extinction below 5 mag and about half below 3 mag, this basically rules out that the candidates too faint for spectroscopy down to  $J \sim 21$  contain a sizable population of planemos. According to the COND and DUSTY isochrones, this limit corresponds to object masses of 0.002-0.003  $M_\odot$  (for  $A_V$  of 0-5 and age of 1 Myr).

#### 5.4. The frequency of planemos

In the following we will use the survey results in NGC1333 to give a quantitative constraint on the frequency of planemos which can be compared with other star forming regions. To do this, we estimate the fraction of brown dwarfs which have a mass in the planemo domain,  $f_P = N_P/N_{BD}$ . This quantity serves as a proxy for the shape of the mass function in the substellar regime. Here we treat the population of planemos as a subsample of the population of brown dwarfs.

Our survey in NGC1333 yields only 3 objects with effective temperatures below 2500 K or spectral types later than M9. According to the currently available 1-5 Myr isochrones these objects have masses below the Deuterium burning limit of 0.015  $M_\odot$  and are thus good candidates for planemos. As outlined above, we might miss about 6 more planemos due to our cutoff in the mid-infrared colour.

The total number of brown dwarfs can be calculated as follows: Adding the objects listed in SONYC-IV and this paper, there are 58 with spectral type M5 or later or effective temperatures of 3200 K or below. From these around 10-20 are likely to be above the substellar boundary, which leaves 38-48 brown dwarfs. Following the same statistical arguments that we have used in Sect. 4.1. of SONYC-IV we estimate that we might miss up to 13 more brown dwarfs, plus 6 planemos (see above), i.e. the total is 57-67.

Thus, for NGC1333 we estimate that  $f_P$  is 12-14%. Just counting the number of confirmed objects, the ratio becomes 6-8%. This includes all planemos down to masses of 0.006-0.008  $M_\odot$  (the mass limit for  $J = 19$  and

$A_V = 5$ ).

This value can be compared with other star forming regions. This comparison comes with three caveats: 1) Only  $\sigma$  Ori and UpSco have been surveyed with a depth comparable to our survey in NGC1333, i.e. all other ratios should be considered lower limits. 2) While the general survey strategy is similar in all cases (candidate selection based on optical/near-infrared photometry plus follow-up spectroscopy), the details of the strategy differ from region to region, which might introduce unknown biases. To be conservative, we focus in the following mostly on samples with spectroscopic confirmation. 3) Most of the studies listed below do not make an attempt to estimate the *total* substellar population, by taking into account possible survey biases.

We note that all existing surveys use the COND/DUSTY isochrones for mass estimates, as in our paper. In the case these isochrones turn out to be systematically off, the results of the comparison should still be valid and merely shifted to different mass regimes.

*$\sigma$  Ori:* The summary paper by Caballero et al. (2007) lists 46 confirmed brown dwarfs, out of which 12 are expected to be in the planemo regime, i.e.  $f_P \sim 26\%$ . Not all of these objects are spectroscopically confirmed, but the contamination in this cluster is generally low due to the negligible extinction. The surveys in this region are similarly deep as in NGC1333, i.e. the numbers should be comparable.

*Upper Scorpius:* Based on photometry and proper motions from UKIDSS, the total number of brown dwarfs in this region is 68 in the UKIDSS covered area, out of which 49 are in the northern area where follow-up spectroscopy is available (Dawson et al. 2011). The currently ongoing spectroscopic verification shows that essentially all these objects are indeed members of UpSco (Lodieu et al. 2008, 2011a). Converting the photometry to masses, this sample should cover the mass range down to 0.01  $M_\odot$  and contains about half a dozen objects below 0.015  $M_\odot$ . A deeper survey by Lodieu et al. (2011b) does not find new members in the planemo domain.<sup>10</sup> This yields  $f_P \sim 10\%$ .

*$\rho$ -Ophiuchus:* This region is affected by very high and variable extinction, which strongly hampers any survey. The existing census is not nearly complete below 0.03  $M_\odot$ . So far, there are around 40 confirmed objects with spectral types later or equal M6 from Wilking et al. (2008); Geers et al. (2011); Marsh et al. (2010a); Mužić et al. (2012); Alves de Oliveira et al. (2010, 2012). Out of these, 8 might be in the planemo regime based on spectral type and effective temperature, which results in  $f_P \sim 20\%$ .

*Chamaeleon-I:* The census by Luhman (2007); Luhman & Muench (2008) contains 35 objects with spectral type of M6 or later which are to be considered brown dwarfs. 5 of these have estimated masses below 0.015  $M_\odot$ , i.e.  $f_P \sim 14\%$ . We note that our own deep survey work in Cha-I has not revealed any additional planemos yet down to 0.008  $M_\odot$  (Mužić et al. 2011).

Taking into account the caveats listed above, the val-

<sup>10</sup> Here we neglect the 5 T-dwarf candidates identified based on imaging in Methane-sensitive narrow-band filters without spectroscopic or proper motion confirmation.

ues for  $f_P$  in the various regions are consistent with each other and in the range between 10 and 20%; only  $\sigma$  Ori might have a slightly larger planemo fraction. Focusing on the confirmed objects, NGC1333 has a relatively low planemo fraction compared with other star forming areas.

We can also estimate the fraction of planemos with respect to the population of young stars,  $g_P = N_P/N_S$ . For NGC1333 we have recently determined that the star-vs-brown dwarf ratio, defined as  $R_1 = N(0.08 - 1.0 M_\odot)/N(0.03 - 0.08 M_\odot)$ , is  $2.3 \pm 0.5$ , for most other regions this ratio is larger. Taking this into account, for NGC1333 the fraction of planemos with respect to the total cluster population is in the range of 2-3%. For the other regions where this type of census is available this number becomes 2-5%, i.e. stars are 20-50 times more frequent than planemos. This is consistent with the planemo fraction of  $< 10\%$  (Lucas et al. 2005) and 1-14% (Lucas et al. 2006) derived for the Orion Nebulae Cluster (ONC), albeit for slightly different mass limits. Thus, the number of planemos is insignificant compared with the total population of stars and brown dwarfs. The planemo contribution to the mass budget of young clusters is negligible (well below 1%).

### 5.5. The mass spectrum

With the available database of spectroscopically confirmed objects in NGC1333, we are in the position to construct the Initial Mass Function (IMF) in the low-mass regime. We choose to express the IMF as a mass spectrum  $dN/dM \propto M^{-\alpha}$ . To do that, we use the same spectroscopic samples as in Sect. 5.1, combining the confirmed low-mass stars from Winston et al. (2009) with the census of very low mass objects. We select all M and L dwarfs, in total 107 objects, out of which 100 have an estimate for the effective temperature, either from our survey or from Winston et al. (2009).

Masses were derived for this sample by comparing the temperatures with theoretical evolutionary tracks. Temperatures do not significantly depend on age in the 1-10 Myr phase, as opposed to luminosities and magnitudes, and thus provide a mass estimate that is insensitive to age spread. We use the 1 Myr isochrone from the BCAH models for  $M \geq 0.1 M_\odot$  and the 1 Myr isochrone from the DUSTY models for  $M < 0.1 M_\odot$ . For each object with a given  $T_{\text{eff}}$ , we selected the isochrone datapoints within  $\pm 200$  K around  $T_{\text{eff}}$ , fitted this section either linearly (if there are less than 5 datapoints) or with a second order polynomial, and used that function to calculate the mass corresponding to  $T_{\text{eff}}$ . All masses are tied to this isochrone and should not be compared with values derived using other models.

The mass spectrum was calculated in a way to achieve similar statistical uncertainties in each mass bin, i.e. with varying bin size. For  $M > 0.7 M_\odot$  the sample sizes are too small for a meaningful analysis, the 10 objects above this limit were excluded. The lowest mass bin includes all objects with  $M < 0.03 M_\odot$ . In Fig. 11 we plot our result. The datapoints in this diagram are consistent with  $dN/dM \propto M^{-\alpha}$  with  $\alpha = 0.61$ , overplotted as dashed line. For the substellar regime alone, the best-fitting slope is  $\alpha = 0.46$ . For the stellar regime above  $0.1 M_\odot$  the slope becomes  $\alpha = 1.0$ . The uncertainty in the slope is in the range of 0.1.

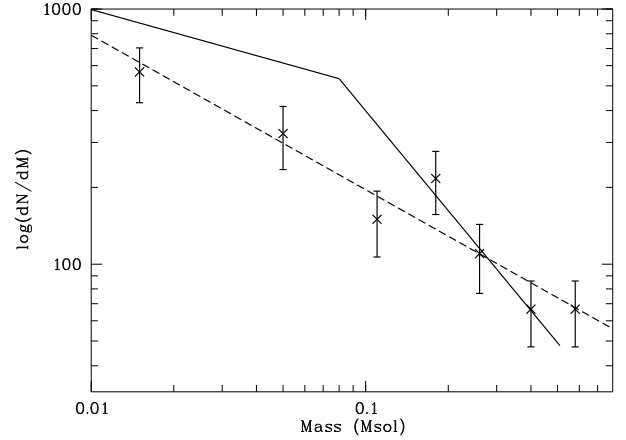


FIG. 11.— Mass function in NGC1333 based on the spectroscopically confirmed members with measured effective temperatures. The binsizes were chosen to achieve approximately equal error bars. The solid lines show the Kroupa mass function ( $\alpha = 1.3$  for  $0.08 < M < 0.5 M_\odot$ ,  $\alpha = 0.3$  for  $M < 0.08 M_\odot$ ). The dashed line shows the best fit to the data ( $\alpha = 0.6$ ).

To verify how the uncertainties in the effective temperatures ( $\pm 200$  K) affect these results, we carried out the following test: For half the objects, randomly selected, we increased  $T_{\text{eff}}$  by 200 K, for the other half we reduced it by 200 K. This effectively scrambles the values within the errorbars. Then the mass spectrum was calculated again using the same procedure. This yields  $\alpha = 0.66$  for the entire sample and 0.55 for the brown dwarfs, slightly higher as before but well within the errorbars. This test also shows that the peak around  $0.2 M_\odot$  seen in the figure is spurious.

Also shown is the Kroupa IMF, an empirical description of the mass spectrum as a segmented power law, as a solid line (Kroupa 2001). This function follows  $\alpha = 1.3 \pm 0.5$  in the stellar regime up to  $0.5 M_\odot$  and  $\alpha = 0.3 \pm 0.7$  in the substellar domain. Within the uncertainties, the Kroupa IMF is consistent with the mass spectrum in NGC1333.

The slope derived here is broadly consistent with values derived for most other star forming regions and young clusters. Some examples: For the very low mass objects in  $\sigma$  Ori, values of 0.6-0.7 have been published in the literature (Caballero et al. 2007; Béjar et al. 2011). For the domain from  $0.03$  to  $0.6 M_\odot$  the cluster Blanco 1 has a mass function with  $\alpha = 0.69 \pm 0.15$  (Moraux et al. 2007). For Upper Scorpius and the mass regime  $0.01$ - $0.3 M_\odot$ , a value of  $\alpha = 0.6 \pm 0.1$  has been published (Lodieu et al. 2007). For the Pleiades  $\alpha$  is found to be in the range of 0.6-1.0 in the low-mass regime (e.g. Moraux et al. 2003, and references therein). For the  $\alpha$  Per cluster, the slope is  $0.59 \pm 0.05$  (Barrado y Navascués et al. 2002). In Collinder 69 the slope has been found to be between 0.2 and 0.4 for the low-mass regime (Bayo et al. 2011).

To our knowledge, the only young region where a significantly different slope of the mass spectrum has been determined is the Orion Nebulae Cluster. In a recent paper, Da Rio et al. (2011) find  $\Gamma$  of  $-1.1$  to  $-3.1$  for the substellar regime, which corresponds to a negative  $\alpha$  ( $\alpha = \Gamma + 1$ ). Similar results have been found in previous studies in the ONC (e.g. Muench et al. 2002). These numbers appear to be anomalous compared with

the other regions mentioned above.

Apart from the overall slope, we can examine the shape of the mass spectrum in NGC1333. In equal sized bins, the numbers per bin increase continuously with decreasing mass, with the exception of a slight minimum around  $0.1\text{--}0.2 M_\odot$ . However, the test with the modified temperatures (see above) indicates that this minimum is spurious, the data is indeed consistent with a monotonically rising histogram. The same result has been obtained for Upper Scorpius and  $\sigma$  Ori, while some other regions show a peak in the mass spectrum around  $0.1\text{--}0.2 M_\odot$  and a smaller slope for lower masses (IC348, Cha-I,  $\rho$ -Oph, Luhman 2007; Alves de Oliveira et al. 2012). One consequence of this difference is a smaller star-to-brown-dwarf ratio (i.e. a large number of brown dwarfs relative to stars) in regions with monotonically rising mass spectrum – as it is indeed found for NGC1333. As discussed in SONYC-IV, a comparison of these ratios possibly indicates environmental differences in the formation of brown dwarfs.

The focus of this study is the planetary mass domain. Assuming a monotonic continuation of the power law shown in Fig. 11 with  $\alpha = 0.6 \pm 0.1$ , we would expect  $8 \pm 3$  objects with  $0.005 < M < 0.015 M_\odot$ , i.e. in the planemo domain and detectable in our survey. For comparison, in Sect. 5.3 we derive an upper limit of 8 planemos in this mass regime from our survey, taking into account the incompleteness in the spectroscopic follow-up of our candidates. Thus, the data is consistent with a monotonic power law mass spectrum across the Deuterium burning limit, but a smaller slope is possible as well. Our survey rules out that the slope of the mass spectrum in NGC1333 increases in the planemo regime.

Again this is in agreement with previous findings for other regions. In  $\sigma$  Ori the census of substellar objects is well approximated by a monotonic slope down to planetary masses (Caballero et al. 2007; Béjar et al. 2011; Peña Ramírez et al. 2012), with a possible turnover (i.e. a lower  $\alpha$ ) in the mass spectrum below  $0.006 M_\odot$ . For Upper Scorpius, the results by Lodieu et al. (2011b) favour a turndown below  $0.01 M_\odot$ . We note that Marsh et al. (2010b) show a mass function of  $\rho$ -Ophiuchus covering the entire planemo regime based on a photometrically selected candidate sample, which resembles the one in  $\sigma$  Ori. Taken together, it seems safe to conclude that the slope of the mass function in the planemo domain is  $\alpha \lesssim 0.6$ .

We note that  $\alpha \lesssim 0.6$  corresponds to a planemo fraction as defined in Sect. 5.4 of  $f_P \lesssim 20\%$  (if the entire planemo domain is considered) or  $f_P \lesssim 30\%$  (with an lower mass cutoff at  $0.005 M_\odot$ ). Indeed, no regions shows a larger planemo fraction, most surveys indicate significantly lower values, including our own work in NGC1333.

Thus, the current census of star forming regions provides support for the idea that planemos are an extension of the population of stars and brown dwarfs and form through the same mechanisms. The observations indicate that free-floating objects with planetary masses exist down to at least  $0.006 M_\odot$ , but, as pointed out in Sect. 5.4, their numbers and their mass budget are insignificant compared with the total population of stars and brown dwarfs.

Some theoretical estimates for the lower mass limit in the star formation process – the opacity limit for

fragmentation – are  $0.007$  (Low & Lynden-Bell 1976) or  $0.01 M_\odot$  (Silk 1977) from analytical arguments and  $< 0.001$  (Boss 2001) or  $0.003\text{--}0.009 M_\odot$  (Bate 2005) from numerical simulations. Except for the lowest-mass values, all these estimates are consistent with the current observational picture.

Sumi et al. (2011) recently determined the slope of the mass spectrum based on microlensing surveys, and find  $1.3 \pm 0.3$  for  $M < 0.01 M_\odot$ , significantly higher than for brown dwarfs ( $0.49$  in their work), indicating that Jupiter-mass objects are almost twice as common as stars. Their estimate includes planetary-mass objects without host stars (i.e. free-floating) and those on wide orbits, but they argue that the majority of them are indeed unbound (but see Quanz et al. (2012) for a criticism of this claim). This is in clear disagreement with the results from the surveys in star forming regions, where the number of planemos per star is much smaller (see Sect. 5.4) and the slope in the mass spectrum is not rising (see above). If the microlensing result holds, the additional planemos would have to be in the mass regime  $< 0.005 M_\odot$  which is not sufficiently probed by the cluster surveys. This would imply a break in the slope of the mass spectrum in the planemo domain, favouring a scenario where the Jupiter-mass objects form in a different way than the planemos and brown dwarfs seen in the star forming regions – as indeed concluded by Sumi et al. (2011). Larger samples of short-period microlensing events and deeper surveys in star forming regions are critical to understand if they are in fact different populations or not.

In another recent paper, Strigari et al. (2012) estimate that there may be up to  $10^5$  objects with masses between  $10^{-8}$  and  $10^{-2} M_\odot$  (called ‘nomads’ in their paper) per main-sequence star. To arrive at this number, they use the slope of the mass spectrum in the brown dwarf/planemo regime as a constraint. Their upper limit of  $10^5$  can only be obtained by using  $\alpha = 2$ . As shown above, this is inconsistent with the surveys in star forming regions. For a more realistic value of  $\alpha = 0.5$ , the result given in their paper is  $\gtrsim 1$  nomads per main-sequence star. Given the enormous difficulties in extrapolating the mass function over 6 orders of magnitude in mass and different modes of formation, these estimates remain highly speculative.

## 6. CONCLUSIONS

We present new spectroscopy for 19 very faint candidate members in the young cluster NGC1333. 7 of them are confirmed as very low mass objects, most or all of them should be brown dwarfs. Based on the combined spectroscopic follow up from SONYC-I, SONYC-IV and this paper, we are able to put limits on the IMF and the number of free-floating planetary-mass objects (planemos,  $M < 0.015 M_\odot$ ) in this cluster. The mass spectrum is in good agreement with a monotonically rising power law  $dN/dM \propto M^{-\alpha}$ , with  $\alpha = 0.6 \pm 0.1$  for  $M < 0.6 M_\odot$ . The overall slope is in agreement with all previous studies in other regions, with the ONC as only exception.

Among the substellar population in NGC1333 are 3 with estimated masses in the planemo domain. Taking into account the incompleteness of the spectroscopic follow-up in our survey, we estimate that the cluster

could harbour a total of 8 planemos down to masses of  $\sim 0.005 M_{\odot}$ . This translates into a planemo fraction (the fraction of brown dwarfs in the planetary mass domain) of 12-14%. This is comparable to the planemo fractions determined for other regions. We estimate that there are 20-50 times more stars than planemos in young clusters. Based on the constraints on the number of planemos in star forming regions, the slope of the mass spectrum is  $\lesssim 0.6$  below  $0.015 M_{\odot}$ , i.e. it does not increase in the planemo domain. These findings support the idea that planemos form through the same mechanisms as young stars and brown dwarfs.

The authors would like to thank the Subaru staff for the assistance during the observations and their preparation. We thank Jenny Patience for making her spectra available to us. The careful review by an anonymous referee helped us to improve the manuscript. AS acknowledges financial support the grant 10/RFP/AST2780 from the Science Foundation Ireland. The research was supported in large part by grants from the Natural Sciences and Engineering Research Council (NSERC) of Canada to R.J. R.J.'s work was also supported in part by the Radcliffe Institute for Advanced Study at Harvard University.

## REFERENCES

- Allard, F., Hauschildt, P. H., Alexander, D. R., Tamanai, A., & Schweitzer, A. 2001, *ApJ*, 556, 357
- Alves de Oliveira, C., Moraux, E., Bouvier, J., & Bouy, H. 2012, *ArXiv e-prints*
- Alves de Oliveira, C., Moraux, E., Bouvier, J., Bouy, H., Marmo, C., & Albert, L. 2010, *A&A*, 515, A75
- Aspin, C., Sandell, G., & Russell, A. P. G. 1994, *A&AS*, 106, 165
- Baraffe, I., Chabrier, G., Allard, F., & Hauschildt, P. H. 1998, *A&A*, 337, 403
- Baraffe, I., Chabrier, G., Barman, T. S., Allard, F., & Hauschildt, P. H. 2003, *A&A*, 402, 701
- Barrado y Navascués, D., Bouvier, J., Stauffer, J. R., Lodieu, N., & McCaughrean, M. J. 2002, *A&A*, 395, 813
- Bate, M. R. 2005, *MNRAS*, 363, 363
- Bayo, A., Barrado, D., Stauffer, J., Morales-Calderón, M., Melo, C., Huélamo, N., Bouy, H., Stelzer, B., Tamura, M., & Jayawardhana, R. 2011, *A&A*, 536, A63
- Béjar, V. J. S., Zapatero Osorio, M. R., Rebolo, R., Caballero, J. A., Barrado, D., Martín, E. L., Mundt, R., & Bailer-Jones, C. A. L. 2011, *ApJ*, 743, 64
- Belikov, A. N., Kharchenko, N. V., Piskunov, A. E., Schilbach, E., & Scholz, R.-D. 2002, *A&A*, 387, 117
- Boss, A. P. 2001, *ApJ*, 551, L167
- Brandeker, A., Jayawardhana, R., Ivanov, V. D., & Kurtev, R. 2006, *ApJ*, 653, L61
- Caballero, J. A., Béjar, V. J. S., Rebolo, R., Eisloffel, J., Zapatero Osorio, M. R., Mundt, R., Barrado y Navascués, D., Bihain, G., Bailer-Jones, C. A. L., Forveille, T., & Martín, E. L. 2007, *A&A*, 470, 903
- Caballero, J. A., Burgasser, A. J., & Klement, R. 2008, *A&A*, 488, 181
- Chabrier, G., Baraffe, I., Allard, F., & Hauschildt, P. 2000, *ApJ*, 542, 464
- Cushing, M. C., Rayner, J. T., & Vacca, W. D. 2005, *ApJ*, 623, 1115
- Da Rio, N., Robberto, M., Hillenbrand, L. A., Henning, T., & Stassun, K. G. 2011, *ArXiv e-prints*
- Dawson, P., Scholz, A., & Ray, T. P. 2011, *MNRAS*, 418, 1231
- Enoch, M. L., Young, K. E., Glenn, J., Evans, II, N. J., Golwala, S., Sargent, A. I., Harvey, P., Aguirre, J., Goldin, A., Haig, D., Huard, T. L., Lange, A., Laurent, G., Maloney, P., Mauskopf, P., Rossinot, P., & Sayers, J. 2006, *ApJ*, 638, 293
- Evans, N. J., Dunham, M. M., Jørgensen, J. K., Enoch, M. L., Merín, B., van Dishoeck, E. F., Alcalá, J. M., Myers, P. C., Stapelfeldt, K. R., Huard, T. L., Allen, L. E., Harvey, P. M., van Kempen, T., Blake, G. A., Koerner, D. W., Mundy, L. G., Padgett, D. L., & Sargent, A. I. 2009, *ApJS*, 181, 321
- Geers, V., Scholz, A., Jayawardhana, R., Lee, E., Lafrenière, D., & Tamura, M. 2011, *ApJ*, 726, 23
- Gutermuth, R. A., Myers, P. C., Megeath, S. T., Allen, L. E., Pipher, J. L., Muzerolle, J., Porras, A., Winston, E., & Fazio, G. 2008, *ApJ*, 674, 336
- Jayawardhana, R., & Ivanov, V. D. 2006, *ApJ*, 647, L167
- Kroupa, P. 2001, *MNRAS*, 322, 231
- Lada, C. J., Alves, J., & Lada, E. A. 1996, *AJ*, 111, 1964
- Leggett, S. K., Saumon, D., Marley, M. S., Lodders, K., Canty, J., Lucas, P., Smart, R. L., Tinney, C. G., Homeier, D., Allard, F., Burningham, B., Day-Jones, A., Fegley, B., Ishii, M., Jones, H. R. A., Marocco, F., Pinfield, D. J., & Tamura, M. 2012, *ApJ*, 748, 74
- Littlefair, S. P., Naylor, T., Mayne, N. J., Saunders, E., & Jeffries, R. D. 2011, *MNRAS*, 413, L56
- Liu, M. C., Delorme, P., Dupuy, T. J., Bowler, B. P., Albert, L., Artigau, E., Reylé, C., Forveille, T., & Delfosse, X. 2011, *ApJ*, 740, 108
- Lodieu, N., Dobbie, P. D., & Hambly, N. C. 2011a, *A&A*, 527, A24
- Lodieu, N., Hambly, N. C., Dobbie, P. D., Cross, N. J. G., Christensen, L., Martin, E. L., & Valdivielso, L. 2011b, *MNRAS*, 418, 2604
- Lodieu, N., Hambly, N. C., Jameson, R. F., & Hodgkin, S. T. 2008, *MNRAS*, 383, 1385
- Lodieu, N., Hambly, N. C., Jameson, R. F., Hodgkin, S. T., Carraro, G., & Kendall, T. R. 2007, *MNRAS*, 374, 372
- Low, C., & Lynden-Bell, D. 1976, *MNRAS*, 176, 367
- Lucas, P. W., & Roche, P. F. 2000, *MNRAS*, 314, 858
- Lucas, P. W., Roche, P. F., & Tamura, M. 2005, *MNRAS*, 361, 211
- Lucas, P. W., Weights, D. J., Roche, P. F., & Riddick, F. C. 2006, *MNRAS*, 373, L60
- Luhman, K. L. 2007, *ApJS*, 173, 104
- Luhman, K. L., Allen, L. E., Allen, P. R., Gutermuth, R. A., Hartmann, L., Mamajek, E. E., Megeath, S. T., Myers, P. C., & Fazio, G. G. 2008, *ApJ*, 675, 1375
- Luhman, K. L., Mamajek, E. E., Allen, P. R., & Cruz, K. L. 2009, *ApJ*, 703, 399
- Luhman, K. L., & Muench, A. A. 2008, *ApJ*, 684, 654
- Marsh, K. A., Kirkpatrick, J. D., & Plavchan, P. 2010a, *ApJ*, 709, L158
- Marsh, K. A., Plavchan, P., Kirkpatrick, J. D., Lowrance, P. J., Cutri, R. M., & Velusamy, T. 2010b, *ApJ*, 719, 550
- Moraux, E., Bouvier, J., Stauffer, J. R., Barrado y Navascués, D., & Cuillandre, J.-C. 2007, *A&A*, 471, 499
- Moraux, E., Bouvier, J., Stauffer, J. R., & Cuillandre, J.-C. 2003, *A&A*, 400, 891
- Muench, A. A., Lada, E. A., Lada, C. J., & Alves, J. 2002, *ApJ*, 573, 366
- Muzić, K., Scholz, A., Geers, V., Fissel, L., & Jayawardhana, R. 2011, *ApJ*, 732, 86
- Muzić, K., Scholz, A., Geers, V., Jayawardhana, R., & Tamura, M. 2012, *ApJ*, 744, 134
- Oasa, Y., Tamura, M., Sunada, K., & Sugitani, K. 2008, *AJ*, 136, 1372
- Patience, J., King, R. R., De Rosa, R. J., Vigan, A., Witte, S., Rice, E., Helling, C., & Hauschildt, P. 2012, *ArXiv e-prints*
- Peña Ramírez, K., Béjar, V. J. S., Zapatero Osorio, M. R., Petr-Gotzens, M. G., & Martín, E. L. 2012, *ArXiv e-prints*
- Pickles, A. J. 1998, *PASP*, 110, 863
- Quanz, S. P., Lafrenière, D., Meyer, M. R., Reggiani, M. M., & Buenzli, E. 2012, *A&A*, 541, A133
- Ridge, N. A., Schnee, S. L., Goodman, A. A., & Foster, J. B. 2006, *ApJ*, 643, 932
- Scholz, A. 2012, *MNRAS*, 420, 1495
- Scholz, A., Geers, V., Jayawardhana, R., Fissel, L., Lee, E., Lafrenière, D., & Tamura, M. 2009, *ApJ*, 702, 805
- Scholz, A., & Jayawardhana, R. 2008, *ApJ*, 672, L49
- Scholz, A., Muzic, K., Geers, V., Bonavita, M., Jayawardhana, R., & Tamura, M. 2012a, *ApJ*, 744, 6
- Scholz, A., Stelzer, B., Costigan, G., Barrado, D., Eisloffel, J., Lillo-Box, J., Riviere-Marichalar, P., & Stoev, H. 2012b, *MNRAS*, 419, 1271
- Silk, J. 1977, *ApJ*, 214, 152

- Stassun, K. G., Mathieu, R. D., & Valenti, J. A. 2007, *ApJ*, 664, 1154
- Strigari, L. E., Barnabè, M., Marshall, P. J., & Blandford, R. D. 2012, *MNRAS*, 2972
- Sumi, T., Kamiya, K., Bennett, D. P., Bond, I. A., Abe, F., Botzler, C. S., Fukui, A., Furusawa, K., Hearnshaw, J. B., Itow, Y., Kilmartin, P. M., Korpela, A., Lin, W., Ling, C. H., Masuda, K., Matsubara, Y., Miyake, N., Motomura, M., Muraki, Y., Nagaya, M., Nakamura, S., Ohnishi, K., Okumura, T., Perrott, Y. C., Rattenbury, N., Saito, T., Sako, T., Sullivan, D. J., Sweatman, W. L., Tristram, P. J., Udalski, A., Szymański, M. K., Kubiak, M., Pietrzyński, G., Poleski, R., Soszyński, I., Wyrzykowski, L., Ulaczyk, K., & Microlensing Observations in Astrophysics (MOA) Collaboration. 2011, *Nature*, 473, 349
- Tamura, M., Itoh, Y., Oasa, Y., & Nakajima, T. 1998, *Science*, 282, 1095
- Wilking, B. A., Gagné, M., & Allen, L. E. 2008, *Star Formation in the  $\rho$  Ophiuchi Molecular Cloud*, ed. Reipurth, B., 351
- Wilking, B. A., Meyer, M. R., Greene, T. P., Mikhail, A., & Carlson, G. 2004, *AJ*, 127, 1131
- Winston, E., Megeath, S. T., Wolk, S. J., Hernandez, J., Gutermuth, R., Muzerolle, J., Hora, J. L., Covey, K., Allen, L. E., Spitzbart, B., Peterson, D., Myers, P., & Fazio, G. G. 2009, *AJ*, 137, 4777
- Zapatero Osorio, M. R., Béjar, V. J. S., Martín, E. L., Rebolo, R., Barrado y Navascués, D., Bailer-Jones, C. A. L., & Mundt, R. 2000, *Science*, 290, 103

